JOURNAL OF AIRCRAFT
Vol. 41, No. 2, March–April 2004

Comparison of Predicted and Measured Formation Flight Interference Effects

William B. Blake*
U.S. Air Force Research Laboratory, Wright–Patterson Air Force Base, Ohio 45433-7531
and
David R. Gingras†
Bihrle Applied Research, Hampton, Virginia 23666

Results from a wind-tunnel test of two delta-wing aircraft in close proximity are presented and compared with predictions from a vortex lattice method. Large changes in lift, pitching moment, and rolling moment are found on the trail aircraft as it moves laterally relative to the lead aircraft. The magnitude of these changes is reduced as the trail aircraft moves vertically with respect to the lead aircraft. Lift-to-drag ratio of the trail aircraft is increased when the wing tips are slightly overlapped. Wake-induced lift is overpredicted slightly when the aircraft overlap in the spanwise direction. Wake-induced pitching and rolling moments are well predicted. A maximum induced drag reduction of 25% is measured on the trail aircraft, compared with a 40% predicted reduction. Three positional stability derivatives, change in lift and pitching moment with vertical position and change in rolling moment with lateral position, are studied. Predicted boundaries between stable and unstable regions were generally in good agreement with experimentally derived boundaries.

Nomenclature

A	=	aspect ratio
b	=	wing span
C_A	=	axial-force coefficient
C_D	=	drag coefficient
C_{Di}	=	induced drag coefficient
C_{D0}	=	zero-lift drag coefficient
C_L	=	lift coefficient
C_l	=	rolling moment coefficient
C_m	=	pitching-moment coefficient
C_N	=	normal-force coefficient
K_0	=	self-induced drag factor
K_{12}	=	formation flight-induced drag factor
α	=	angle of attack
ΔC_D	=	incremental drag coefficient caused by formation flight
ΔC_L	=	incremental lift coefficient caused by formation flight
ΔC_l	=	incremental rolling moment coefficient caused by formation flight
ΔC_m	=	incremental pitching-moment coefficient caused by formation flight
Δx	=	longitudinal distance, Fig. 2
Δy	=	lateral distance, Fig. 2
Δz	=	vertical distance, Fig. 2

Introduction

MANY military missions involve formation flight. In some instances there is significant aerodynamic coupling between aircraft arising from the proximity of one aircraft to the wakes generated by other aircraft in the formation. Although aerial refueling is the most common example, a new scenario is currently under study—formation flight for drag reduction. This is now considered practical because of the ability to determine aircraft location with high precision and advances in automatic control theory. If the aircraft are correctly positioned, upwash from wing tip vortices can reduce the drag of neighboring aircraft, therefore increasing range or endurance.[1] It is generally accepted that this drag reduction is one of the reasons that many migratory bird species fly in closely spaced flocks.[2] Photographic studies of Canadian geese have found that the average lateral spacing between adjacent birds is very close to the optimum predicted by simple aerodynamic theory.[3]

Most of the research in this area has concentrated on analytical modeling using potential flow techniques.[4,5] Very few experimental results are reported in the open literature. Brown et al.[6] conducted tow tank tests using a 3% scale Boeing 747 model as the wake generator and a generic fighter as the trail aircraft. The trail-to-lead aircraft wing span ratio was 0.20. Forces were measured on the trail aircraft only, with lift-to-drag ratio increases of up to 50% measured at some conditions. Beukenberg and Hummel[7] conducted two flight tests in an attempt to demonstrate a power saving under realistic conditions. In their second test a Dornier-228 acted as a vortex generator for a following Dornier-28. Using an automatic control system to maintain proper position, an average power reduction of 10% was measured on the trail aircraft over a 150-s interval.

There have been many wind-tunnel tests studying the impact of wake vortices on aircraft far downstream. Most of these center on the study of wake vortex hazards for commercial aircraft and are conducted in large facilities.[8,9] Bloy et al.[10] investigated formations typical of aerial refueling with the receiver less than one wing span downstream of the tanker. Their tests were conducted in a small wind tunnel with a relatively large wing-span-to-tunnel-width ratio of 0.7. Significant wall interference effects were uncovered by taking measurements in both open and closed test sections.

The flow survey rig within the NASA Langley Research Center 30×60 Full Scale Wind Tunnel has recently been modified to accommodate an aircraft model with an internal force balance.[11] The present work discusses test results from a formation of two closely spaced tailless aircraft using this rig and compares these with predictions from a vortex lattice method.

Wind-Tunnel Setup

The wind-tunnel tests were conducted in the NASA Langley Research Center Full Scale Wind Tunnel. The test configuration is a Lockheed tail-less aircraft consisting of a 65-deg delta wing with a sawtooth trailing edge with a sweep angles of 25 deg. It is a

Received 21 September 2002; revision received 8 August 2003; accepted for publication 11 August 2003.

*Aerospace Engineer, Air Vehicles Directorate. Associate Fellow AIAA.
†Aerospace Engineer. Senior Member AIAA.

Table 1 Estimated measurement accuracy

Parameter	Accuracy
C_N	0.0032
C_A	0.0012
C_m	0.0008
C_l	0.0004

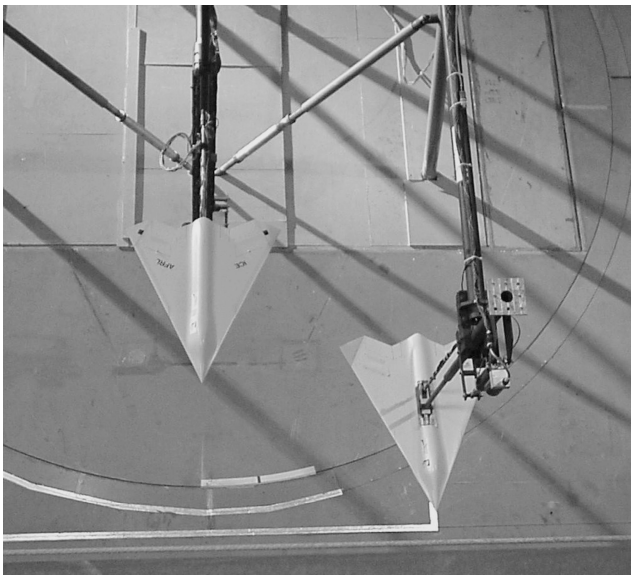

Fig. 1 Wind-tunnel models on apparatus.

single-engine design with two narrow inlets on the lower surface. The inlets were blocked for the present test.

Two 1/13-scale models were tested. These were manufactured several years apart by different firms, so that slight differences are present. They will be referred to as models A and B. Model B was manufactured later and has several bumps and exposed rods to accommodate internally actuated control surfaces. Model B was used as the trail model during all of the formation tests and was mounted using an aft sting, which was connected to a vertical rod. This rod was connected to the wind-tunnel's primary model support system. Model A was mounted from the top on a newly built apparatus, which was attached to the existing flow survey carriage. The apparatus consists of an arm, which projects forward of the survey carriage, under which a vertical sting and angle of attack control rod are attached. This arrangement was selected in an attempt to minimize rig interference effects on model B. A photograph of the experimental apparatus is shown in Fig. 1.

The relative height of the two models is changed by varying the position of model B. This is accomplished by moving the sting along the vertical rod, which is attached to the primary support system. The relative lateral and longitudinal positions are changed by moving the flow survey rig to which model A is attached. All runs are conducted at a tunnel dynamic pressure of 5 psf, which corresponds to a speed of approximately 65 ft/s.

Both models are equipped with internal six component strain-gauge balances. The estimated accuracy of the balance measurements, based on pretest balance calibrations expressed in nondimensional form using the reference area and length of the study vehicle, is presented in Table 1. Additional details on the experimental setup and data reduction are given by Gingras.[11]

Prediction Method

The planar vortex lattice code HASC95[12] is used to predict the wake-induced effects on the trail aircraft. Each aircraft is modeled with 540 panels, using 36 panels in the spanwise direction and 15 panels in the chordwise direction. The spanwise panels are evenly spaced while cosine spacing is used for the chordwise elements. Care was taken to ensure correct alignment of vortex filaments and control

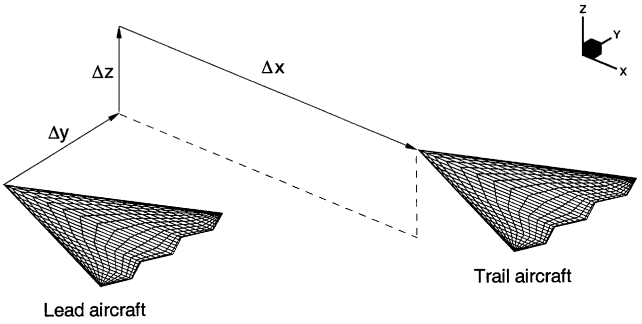

Fig. 2 Vortex lattice representation of vehicles.

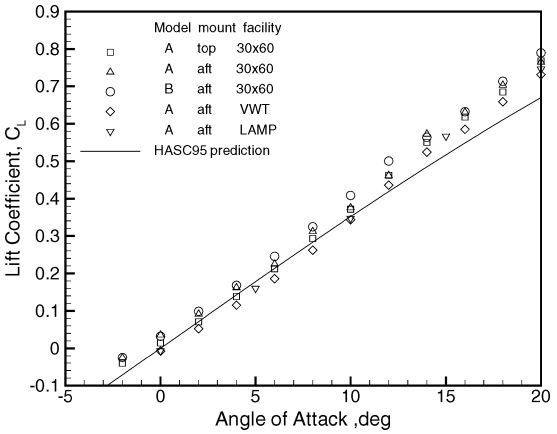

Fig. 3 Lift of models in isolation.

points when the aircraft overlapped in the lateral direction. HASC95 uses a flat wake approximation, that is, the trailing vortex legs extend to infinity parallel to the x–y plane, and do not vary with angle of attack. One result of this is that in the linear lift region the wake-induced lift, rolling-moment and pitching-moment increments are invariant with the angle of attack of the trail aircraft. The HASC95 representation of the vehicles is shown in Fig. 2.

Rossow[13] has shown that the vortex lattice method is extremely accurate for predicting wake-induced effects when the span of the downstream wing is substantially less than that of the wake-generating wing. When the spans of the two wings are comparable, as in the present tests, the accuracy is degraded somewhat, but trends are still very well predicted. The reduction in accuracy is attributed to distortions of the wake cause by the presence of the downstream wing. Bloy et al.[10] also found good agreement when their with vortex lattice predictions are compared to open test-section results.

Isolated Model Results

The measured lift coefficient of models A and B in isolation is shown in Fig. 3, along with the HASC95 prediction. For the formation flight tests a top-mounted sting is used for model A, and an aft mount is used for model B. Model A was also tested in isolation using both aft and top mounts to assess the sting effects and to allow comparison with prior tests, which used an aft-mounted sting. Also shown are the data from two prior tests[14,15] of model A using an aft-mounted sting. The differences between the models are at least as large as any facility or mounting effects. Model B on the aft mount has slightly higher lift than any of the model A configurations. The HASC95 prediction is very good below 10-deg angle of attack and is slightly low at higher angles of attack.

The drag characteristics of the models in isolation and the HASC95 predictions are shown in Fig. 4. HASC95 cannot calculate zero-lift (parasite) drag because it is a potential flow code. To provide a fair comparison of the drag results from HASC95 with the experimental data, the zero-lift drag measured from model B is added to the HASC95 results. The two models show very similar drag results, with model A having a slightly larger drag at zero lift

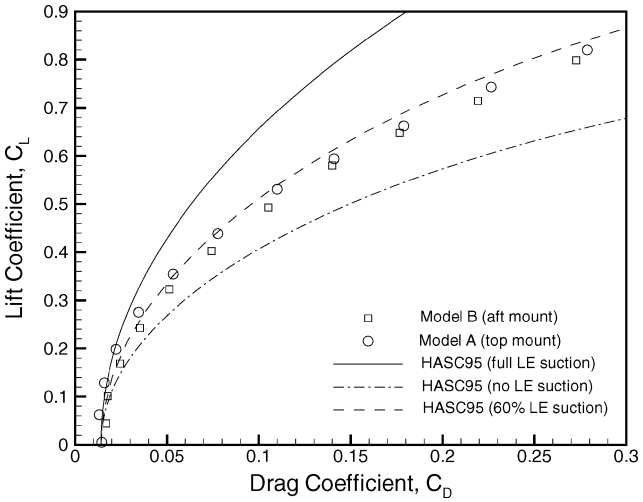

Fig. 4 Drag polars of models in isolation.

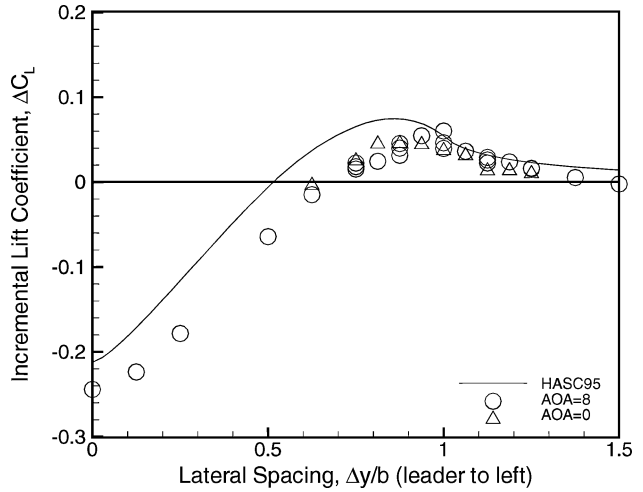

Fig. 5 Effect of lateral spacing on wake induced lift: $\Delta x/b = 2$ and $\Delta z/b = 0$.

than model B. Three predictions are shown, corresponding to three levels of assumed leading-edge suction or flow attachment. Full leading-edge suction corresponds to a fully attached flow condition ($C_{\mathrm{Di}} = C_L^2/\pi A$). Zero leading-edge suction corresponds to a fully separated flow condition ($C_{\mathrm{Di}} = C_L \tan\alpha$). At low lift coefficients the drag compares well with the full suction prediction. As lift increases, some flow separation is evident because of the rise in drag above the full suction prediction. The drag never reaches the value corresponding to fully separated flow case. Several values of suction were run in an attempt to match the value measured at 8 deg angle of attack, which is the reference case for most of the formation-flight effects. A value of 60% attained suction gives a very good match, as shown.

Formation-Flight Results

Lateral Spacing

The effect of lateral spacing on the wake-induced lift is shown in Fig. 5. These results are for a longitudinal spacing of two spans and zero vertical spacing (aircraft in the same plane relative to the oncoming wind). The lead aircraft is at 8 deg angle of attack in all cases. The trail aircraft is at 0 and 8 deg angle of attack. This figure (and several subsequent figures) includes additional data from repeat runs made at lateral spacings of 0.75, 0.875, 1.0, 1.125, and 1.25. The maximum lift loss occurs with the aircraft directly in trail when it is completely enveloped by the downwash from the lead. As the trail aircraft moves outboard, the loss of lift reduces, and upwash is encountered; the effect of upwash reduces once the trail aircraft has passed the lead's wing tip ($\Delta y/b > 1$).

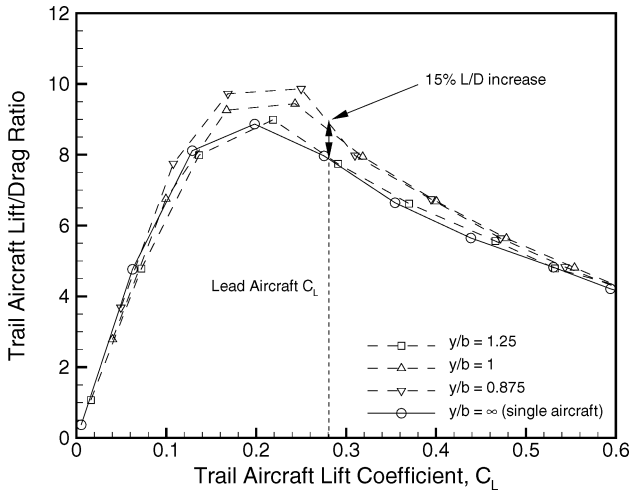

Fig. 6 Formation-flight lift-to-drag characteristics: $\Delta x/b = 2$ and $\Delta z/b = 0$.

The HASC95 prediction shows the correct trend, and the magnitude of the lift is well predicted for lateral spacings greater than $\frac{2}{3}$ span. The loss of lift is underpredicted for smaller spacings. This might be caused by a reduction in local dynamic pressure immediately behind the lead aircraft, which is not accounted for in HASC95. The wake-induced lift is not affected by the angle of attack of the trail vehicle. This is consistent with the HASC95 results.

The lift-to-drag ratio as a function of lift for several lateral spacings is shown in Fig. 6. The aircraft in isolation is shown as the solid line, with formation flight results shown as dashed lines. These data are taken from angle-of-attack sweeps of the trail aircraft with the lead aircraft at a fixed angle of attack. If two similar aircraft fly in formation for an extended period in order to increase range, they need to periodically change position during the flight to keep the fuel loads roughly comparable.[14] On average, they would be at approximately the same weight and corresponding lift coefficient. As a result, the most meaningful drag-reduction comparison is for the case where both aircraft are at the same lift coefficient. Here, a drag reduction of almost 15% is attained for the trail aircraft. Smaller reductions are found if the trail aircraft is at a higher lift coefficient than the lead (or heavier than the lead aircraft), and larger reductions are found if the trail aircraft is at a lower lift coefficient (or lighter than the lead aircraft).

In the HASC95 runs both aircraft are at the same angle of attack, so that the lift of the two vehicles is almost always different. Prandtl's method[16] was used to extract the induced drag effect for cases of differing lift on the lead and trail wings:

$$C_{D,2} = C_{D,0} + K_0 C_{L,2}^2 + K_{12} C_{L,1} C_{L,2} \tag{1}$$

The induced drag change caused by formation effects can be easily calculated:

$$\frac{K_{12}}{K_0} = \frac{C_{L,2}}{C_{L,1}}\left(\frac{C_{D,2} - C_{D,0}}{K_0 C_{L,2}^2} - 1\right) \tag{2}$$

The same procedure is used to extract the induced drag reduction from the experimental data. K_0 is determined from a curve fit of the isolated aircraft lift-and-drag results. If two untapered wings are physically joined, the induced drag change of the added wing (K_{12}/K_0) is -1 or a 100% reduction. The HASC95 results for the fully attached flow case (dashed curve) indicate a maximum reduction of about 70% at a spacing of 90% span, indicating a slight overlap of the wings. Simple horseshoe vortex theory predicts a maximum reduction of 100% at $\pi/4$(78%) span. The reduction is smaller for the present case because of the high degree of wing taper. The HASC95 results for 60% attained suction show a predicted drag reduction of 40% at 90% span spacing. The test data show that a maximum reduction of about 25% occurs between 80 and 90%

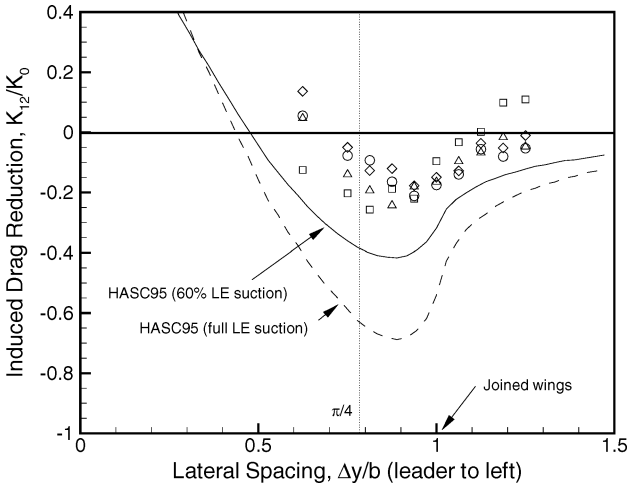

Fig. 7 Effect of lateral spacing on induced drag reduction: $\Delta x/b = 2$ and $\Delta z/b = 0$.

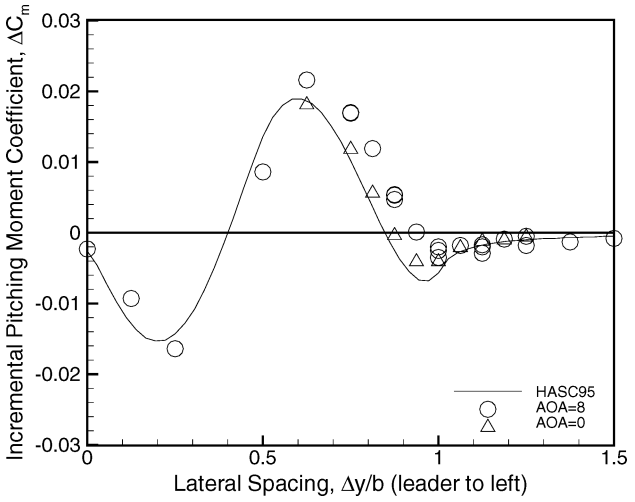

Fig. 8 Effect of lateral spacing on wake-induced pitching moment: $\Delta x/b = 2$ and $\Delta z/b = 0$.

span spacing. Although the overall trend of the data matches the prediction, the reduction is about 15% less than predicted at all lateral spacings. One possible explanation for this discrepancy is that the induced velocities at the trail aircraft wing tip are high enough to significantly increase flow separation. Using a pair of fully rolled-up vortices to represent the wake, the estimated induced upwash angle at the tip of the trail aircraft is 8 deg for the present test conditions. Added to the geometric angle of attack of 4–10 deg, this almost certainly increases separation.

The effect of lateral spacing on the wake-induced pitching moment is shown in Fig. 8. For reference, a maximum (30-deg) elevon deflection gives a pitching-moment increment of -0.040, so that the maximum induced moment corresponds to about a 50% control deflection. There are three distinct peaks in the incremental moment, which occur at spacings of approximately one-quarter span, two-thirds span, and wing tip. HASC95 does an excellent job of predicting the size and location of these peaks. The pitching moment data in Fig. 8 show a small effect of angle of attack when the wings overlap ($\Delta y/b < 1$), with an increased nose-up moment with angle of attack. The zero-angle-of-attack data are more accurately predicted by HASC95. If it is assumed that the wake from the lead is parallel to the velocity vector, then at zero angle of attack the trail aircraft is perfectly aligned with the lead's wake, which is the HASC95 representation.

To examine the changes in sign of the pitching-moment result, pressure distributions were obtained from HASC95. The pressure

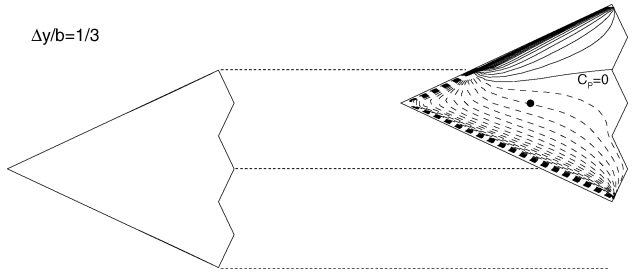

Fig. 9 Wake-induced pressure contours at $\Delta y/b = 1/3$, $\Delta x/b = 2$, and $\Delta z/b = 0$.

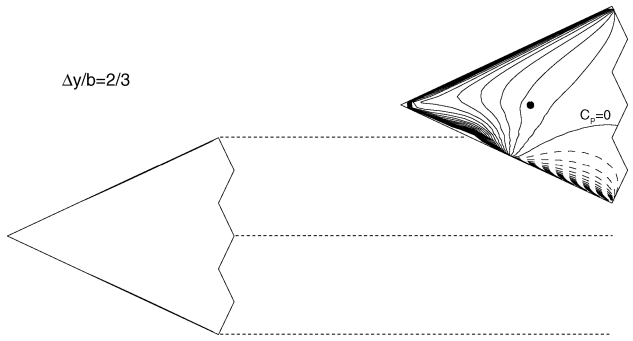

Fig. 10 Wake-induced pressure contours at $\Delta y/b = 2/3$, $\Delta x/b = 2$, and $\Delta z/b = 0$.

distributions are shown for lateral spacings of $\frac{1}{3}$ and $\frac{2}{3}$ span in Figs. 9 and 10. They are obtained by subtracting the pressures of an isolated vehicle at 8 deg angle of attack from the pressures of both vehicles while in formation flight. The dashed curves indicate regions of downwash while solid lines indicate upwash. The contours are shown at increments of 0.02 in terms of Cp. Although there is a small effect of the trail aircraft on the lead, it cannot be seen at this resolution in Cp. The black dots indicate the moment reference center. Figure 9 shows a downwash region that is nearly aligned with the lead aircraft's right wing tip. The upwash is mostly aft of the moment center, with a large downwash at the nose. This results in the nose down moment shown in Fig. 8. Figure 10 shows a small downwash region at the left wing tip of the trail, with only upwash forward of the moment reference center. This results in the maximum nose up moment peak shown in Fig. 8. The approximate dividing line between downwash and upwash for the $\frac{2}{3}$-span case is not aligned with the lead aircraft's wing tip, but at a point further inboard.

The effect of lateral spacing on the wake-induced rolling moment is shown in Fig. 11. For reference, a maximum (30-deg) elevon deflection gives a rolling-moment increment of -0.022, so that the maximum induced moment corresponds to about a 100% control deflection.

Vertical Spacing

The effect of vertical spacing on the wake-induced lift is shown in Fig. 12. Results are shown for a longitudinal spacing of two spans and lateral spacings of 0.25, 0.75, and 1.25 spans. Both the lead and trail aircraft are at 8 deg angle of attack. The scale of the vertical axis matches that shown in Fig. 5 for the lateral spacing comparisons. The trends are very well predicted, while the magnitudes are not. In all cases the maximum lift changes correspond to the in plane ($\Delta z/b = 0$). For some of the 0.75-span results, the same position was tested during multiple runs. These additional points are very close to one another, indicating good repeatability of the induced effects.

The effect of vertical spacing on the wake-induced pitching and rolling moments are shown in Figs. 13 and 14. For the most part, as with the lift, the maximum changes occur for the in-plane case. The pitching-moment results are very well predicted in all cases. The

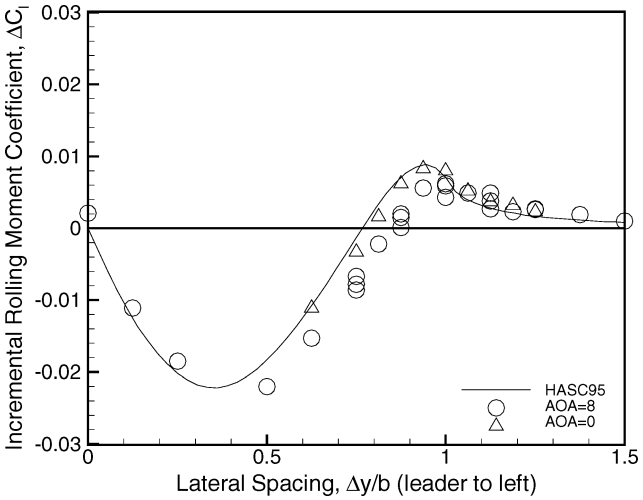

Fig. 11 Effect of lateral spacing on wake-induced rolling moment: $\Delta x/b = 2$ and $\Delta z/b = 0$.

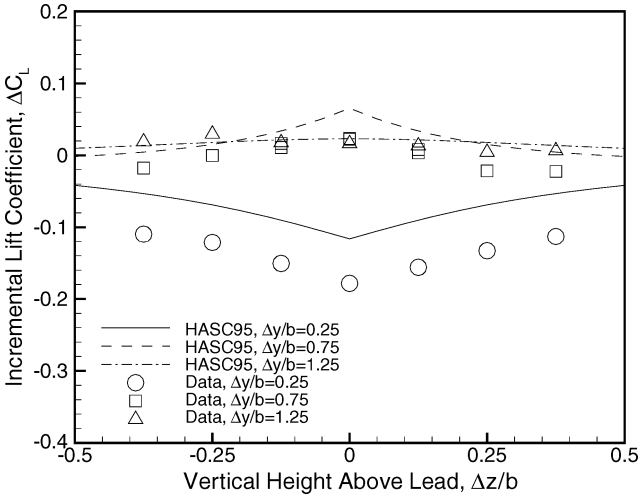

Fig. 12 Effect of vertical spacing on wake-induced lift: $\Delta x/b = 2$.

rolling-moment results are well predicted for the 0.25- and 1.25-span spacing cases. For the 0.75-span case the results are mixed. The data show a continually increasing moment with vertical spacing, whereas the prediction shows virtually no effect of vertical spacing.

Positional Stability

One important aspect of formation flight is positional stability. Positive stability results if the wake-induced forces tend to return the trail aircraft to its original position when disturbed. About a dozen positional stability derivatives exist, many of which have been studied by Bloy et al.[10] For the current tests three stability derivatives are examined, change in lift and pitching moment with vertical spacing, and change in roll with lateral separation. For the sign convention selected, these derivatives are stable for

$$\frac{\partial C_L}{\partial z} < 0, \qquad \frac{\partial C_m}{\partial z} < 0, \qquad \frac{\partial C_l}{\partial y} < 0 \tag{3}$$

The derivatives involving yawing moment and side force were effectively zero as a result of the tailless configuration. Limitations in the experimental apparatus prevented study of other derivatives such as change in roll with bank angle.

The stability boundaries derived from HASC95 for the change in lift with vertical spacing are shown in Fig. 15. The boundaries extracted from the experimental data are shown in Fig. 16. Only data with the trail aircraft to the right of the lead aircraft are shown because this is where the bulk of the data were taken. The boundaries are symmetric with respect to the vertical plane of symmetry of the lead aircraft.

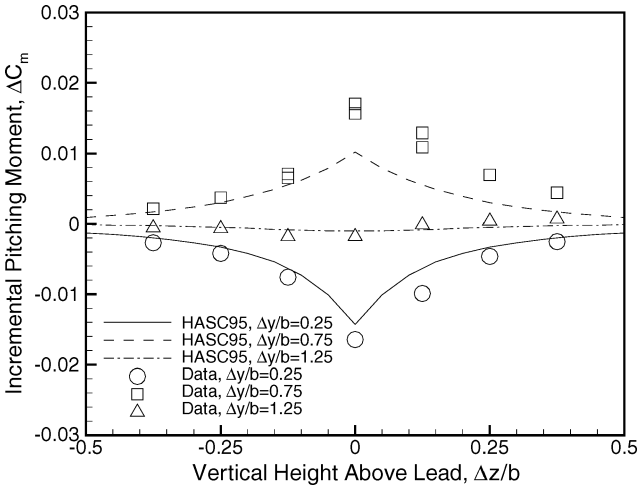

Fig. 13 Effect of vertical spacing on wake-induced pitching moment: $\Delta x/b = 2$.

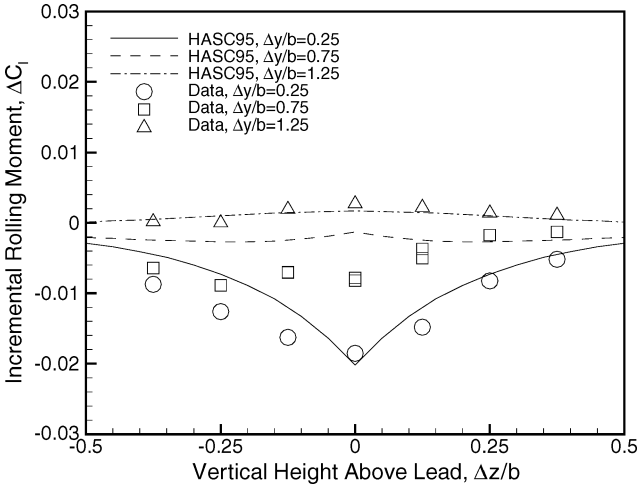

Fig. 14 Effect of vertical spacing on wake-induced rolling moment: $\Delta x/b = 2$.

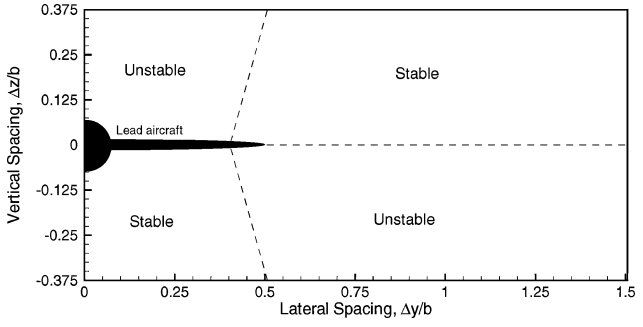

Fig. 15 Predicted regions of positional stability in lift: $\Delta x/b = 2$.

HASC95 predicts four distinct regions of lift stability, stable in lift when the trail aircraft is behind and below the lead aircraft or when it is to the side and above of the lead aircraft. These regions are divided by a four-corner boundary, located at 0.40-span spacing. The measured data agree well with the predicted boundaries with two small exceptions. Instead of a four-corner boundary between regions, the data show the region of positive stability to be continuous with a small region of positive stability present just outside the wing tip ($\Delta y/b = 0.6$). The data also show a small stable region beneath the vertical plane of symmetry outboard of wing tip ($\Delta y/b = 0.6$) spacing.

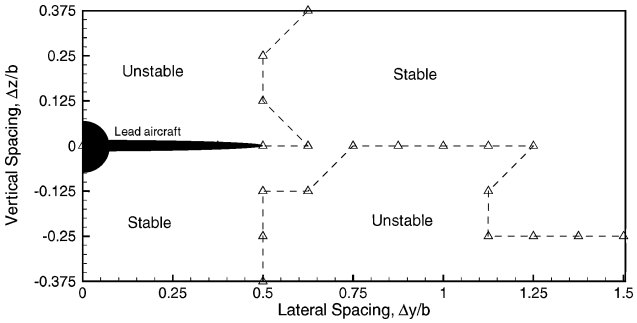

Fig. 16 Measured regions of positional stability in lift: $\Delta x/b = 2$.

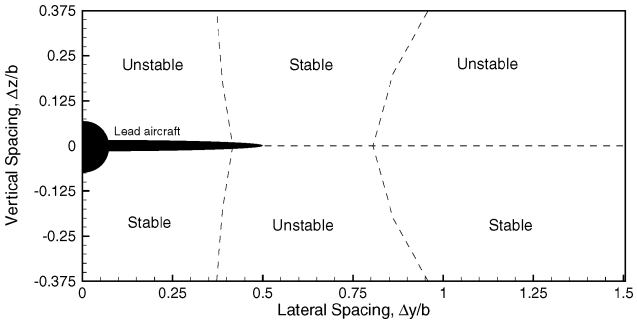

Fig. 17 Predicted regions of positional stability in pitch: $\Delta x/b = 2$.

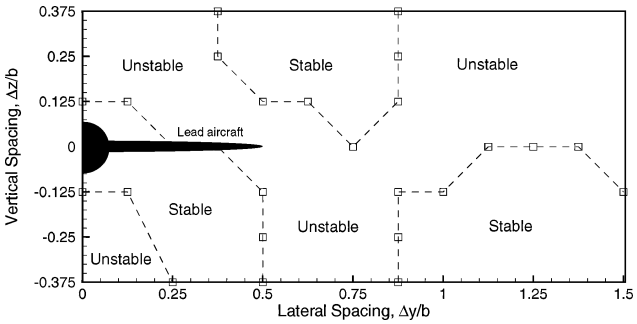

Fig. 18 Measured regions of positional stability in pitch: $\Delta x/b = 2$.

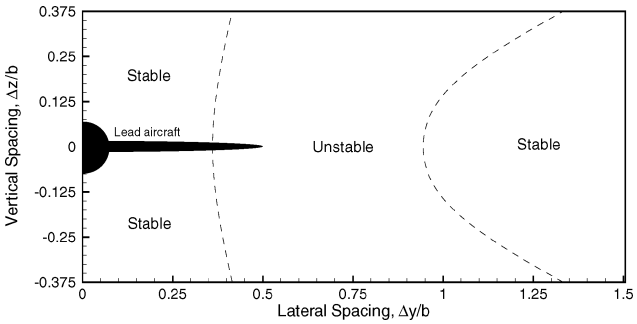

Fig. 19 Predicted regions of positional stability in roll: $\Delta x/b = 2$.

Stability boundaries for the change in pitching moment with vertical spacing are shown in Figs. 17 and 18. HASC95 predicts six distinct stability regions, which are separated by two four-corner boundaries, located at 0.40- and 0.80-span spacing. The data show the same general trends as the prediction. As with the lift prediction, the data do not show four-corner boundaries. Instead, the region of instability is continuous with regions of instability separating the stable regions. In addition, the data show a small region of instability directly behind and below the aircraft that is not predicted.

Stability boundaries for the change in rolling moment with lateral position are shown in Figs. 19 and 20. HASC95 predicts three

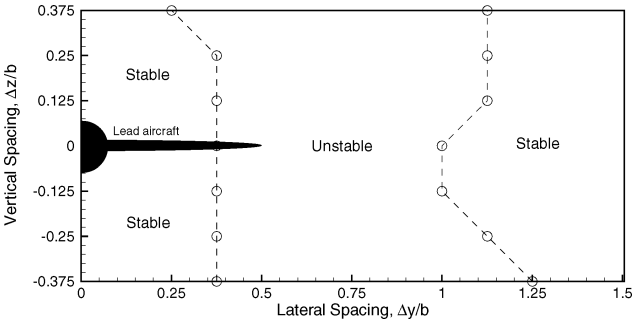

Fig. 20 Measured regions of positional stability in roll: $\Delta x/b = 2$.

distinct stability regions. The boundaries of these regions in the horizontal plane of symmetry are located at 0.36- and 0.94-span spacing. The experimental data agree very well with the prediction. In all three cases there is a break in the stable regions at about 0.40-span spacing. For the basic horseshoe vortex model of a wing, this is the spacing where vortex systems of the wing no longer overlap in the spanwise direction, that is, the trailing vortex of the downstream wing moves outboard of the trailing vortex of the wing upstream.

Conclusions

The results of a wind-tunnel test of two vertical tail-less delta-wing aircraft in close proximity have been presented and compared with predictions from a planar vortex lattice method. The relative positions of the aircraft were varied in the spanwise and vertical directions at a longitudinal separation of two wing spans from nose to nose. Wake-induced effects on lift are observed to be large and well predicted except when the aircraft overlap in the spanwise direction. In that case the lift increments are overpredicted. Wake-induced effects on pitching and rolling moment are large and well predicted in all cases. Wake-induced effects on side force and yawing moment are small, presumably because of the absence of a vertical tail. The induced drag on the trail aircraft is reduced when the aircraft wing tips are aligned or slightly overlap. Drag increases are found when the wing tips overlap by more than 50% span. A maximum induced drag reduction of 25% is measured on the trail aircraft with a wing tip overlap of 15–20% span. This compares with a predicted reduction of 40% with 10% overlap. This discrepancy is attributed to flow separation at the tip caused by upwash. Three positional stability derivatives, change in lift and pitching moment with vertical position and change in rolling moment with lateral position, are studied. Excellent agreement is found between predicted and experimentally derived stability boundaries for the lift and rolling-moment derivative, whereas fair agreement is found for the pitching-moment derivative.

References

[1]Hoerner, S. F., "Fluid Dynamic Drag," published by the author, Bricktown, NJ, 1965.

[2]Lissaman, P. B. S., and Shollenberger, C. A., "Formation Flight of Birds," *Science*, Vol. 168, May 1970, pp. 1003–1005.

[3]Hainsworth, F. R., "Precision and Dynamics of Positioning by Canada Geese Flying in Formation," *Journal of Experimental Biology*, Vol. 128, March 1987, pp. 445–462.

[4]Maskew, B., "Formation Flying Benefits Based on Vortex Lattice Calculations," NASA CR-151974, May 1977.

[5]Blake, W. B., and Multhopp, D., "Design, Performance and Modeling Considerations for Close Formation Flight," AIAA Paper 98-4343, Aug. 1998.

[6]Brown, C. E., Van Dyke, P., and Kloetzli, J. W., "Measurements and Analysis of the Forces Acting on a Small Aircraft Flying in the Upwash of a Large Aircraft," Tracor Hydronautics, TR 7615, Laurel, MD, April 1978.

[7]Beukenberg, M., and Hummel, D., "Aerodynamics, Performance and Control of Airplanes in Formation Flight," International Council of the Aeronautical Sciences, Paper 90-5.9.3, Sept. 1990.

[8]Rossow, V. J., Sacco, J. N., Askins, P. A., Bisbee, L. S., and Smith, S. M., "Measurements in 80 by 120 Foot Wind Tunnel of Hazard Posed by Lift-Generated Wakes," *Journal of Aircraft*, Vol. 32, No. 2, 1993, pp. 278–284.

[9]Pete, K. R., Smith, S. T., and Vicroy, D. D., "Model Validation of Wake-Vortex/Aircraft Encounters," AIAA Paper 2000-3979, Aug. 2000.
[10]Bloy, A. W., West, M. G., Lea, K. A., and Jouma'a, M., "Lateral Aerodynamic Interference Between Tanker and Receiver in Air-to-Air Refueling," *Journal of Aircraft*, Vol. 30, No. 5, 1993, pp. 705–710.
[11]Gingras, D. R., "Experimental Investigation of a Multi-Aircraft Formation," AIAA Paper 99-3143, June–July 1999.
[12]Albright, A. E., Dixon, C. J., and Hegedus, M. C., "Modification and Validation of Conceptual Design Aerodynamic Prediction Method HASC95 with VTXCHN," NASA CR-4712, March 1996.
[13]Rossow, V. J., "Validation of Vortex-Lattice Method for Loads on Wings in Lift-Generated Wakes," *Journal of Aircraft*, Vol. 32, No. 6, 1995, pp. 1254–1262.
[14]Addington, G. A., and Myatt, J. H., "Control Surface Deflection Effects on Aerodynamic Response Nonlinearities," AIAA Paper 2000-4107, Aug. 2000.
[15]Gillard, W. J., and Dorsett, K. M., "Directional Control for Tailless Aircraft Using All Moving Wing Tips," AIAA Paper 97-3487, Aug. 1997.
[16]Prandtl, L., "Induced Drag of Multiplanes," NACA TN 182, March 1924.